Functional Linear Analysis of *in situ* Hyperspectral Data for Assessing CDOM in Rivers

Winner of the AAG-RSSG 2010 Best Paper Award for Early Career Scholars in Remote Sensing[1]
Qian Yu, Yong Q. Tian, Robert F. Chen, Anna Liu, G. Bernard Gardner, and Weining Zhu

Abstract

Turbidity and chlorophyll introduce high uncertainty in remote sensing of Chromophoric Dissolved Organic Matter (CDOM) in riverine and coastal water. To reduce the uncertainty, we developed a functional linear model (FLM) to analyze spectral responses to CDOM concentrations observed in a cruise along two rivers and a tidal bay. The analysis was supported with the measurement of high spatial resolution underwater CDOM concentrations and concurrent in situ above-surface hyperspectral remote sensing reflectance. The functional linear model is able to explain up to 91percent of CDOM observations (R^2 = 0.91, RMSE = 0.0206). The dummy variables of local environmental factors included in the estimation improve CDOM assessment in coastal water. Our analysis suggests that the pattern changes of the FLM coefficient curves provide useful information for understanding the spectral signal interference from turbidity and chlorophyll. This work presents a feasibility study of in situ remote sensing of CDOM on a shipboard platform.

Introduction

Riverine water constituents are influenced predominantly by adjacent terrestrial ecosystems (Bricaud *et al.*, 1981). Chromophoric or colored dissolved organic matter (CDOM) is an important component in riverine water. CDOM can have significant effects on biological activity in aquatic systems by diminishing light penetration, and consequently, influencing bacterial respiration. These properties have limiting effects on photosynthesis of phytoplankton, decreasing primary productivity and affecting ecosystem structure (Hansell and Carlson, 2002). In addition, many observations have provided evidence that CDOM is correlated to dissolved organic carbon (DOC) in many situations (Ferrari *et al.*, 1996; Del Castillo *et al.*, 2000; Stedmon *et al.*, 2006). CDOM is commonly used as an important indicator for DOC dynamics in freshwater and coastal marine ecosystems. CDOM affects the overall water color (rivers, lakes, and ocean) as seen by many satellite remote sensing instruments, such as MODIS and SeaWiFS (Antoine *et al.*, 2008). Therefore, remote sensing of CDOM is important in studying aquatic ecology and carbon dynamics (Ritchie *et al.*, 2003; Mannino *et al.*, 2008).

Many successful research results on remote sensing of CDOM to assess DOC in aquatic ecosystems have been reported by Del Castillo and Miller (2008), Spencer *et al.* (2007), and Vignudelli *et al.* (2004). Currently remote sensing of CDOM has been mostly focused on either lake freshwater (Kutser *et al.*, 2005a; Kutser *et al.*, 2005b) or oceanic marine (Case 1 water) ecosystems (Mobley, 1999; Siegel *et al.*, 2002). Kutser *et al.* (2005b) concluded that CDOM content in lakes in Southern Finland can be estimated by band ratio of EO-1 ALI band 2 and band 3. Other coarser spatial resolution sensors for retrieving CDOM in oceanic and coastal waters are MODIS and SeaWiFS (Mueller and Austin, 1992; Antoine *et al.*, 2008; Brown *et al.*, 2008). A representative algorithm for remote sensing of CDOM, expressed by an absorption coefficient of ocean water is the multi-band quasi-analytical algorithm (QAA) developed by Lee *et al.* (2002). There are several alternative algorithms for remote sensing of CDOM, such as computer-based discrete modeling methods. However, Kishino *et al.* (2005) found that result is unreliable when a Neural Network model was implemented to compute the CDOM concentration using ASTER data from Tokyo Bay.

Common remote sensing algorithms in ocean color are mostly based on the band ratios of remote sensing reflectance R_{rs} at several wavelengths in the visible spectrum

[1] This annual award competition was established by the Remote Sensing Specialty Group (RSSG) of the Association of American Geographers (AAG) in recognition of the AAG's 100th anniversary in 2004 and recognizes exemplary research scholarship in remote sensing by post-dectoral students and faculty in Geography and allied fields.

Qian Yu and Weining Zhu are with the Department of Geosciences, University of Massachusetts-Amherst, 611 N. Pleasant St., Amherst, MA 01003 (qyu@geo.umass.edu).

Yong Q. Tian, Robert F. Chen, and G. Bernard Gardner are with the Department of Environmental, Earth and Ocean Sciences, University of Massachusetts-Boston, 100 Morrissey Blvd., Boston, MA 02125.

Anna Liu is with the Department of Mathematics and Statistics, University of Massachusetts-Amherst, Amherst, MA 01003.

Photogrammetric Engineering & Remote Sensing
Vol. 76, No. 10, October 2010, pp. 1147–1158.

0099-1112/10/7610–1147/$3.00/0

(Brown *et al.*, 2008; Lee and Hu, 2006; Mueller and Austin, 1992). The CDOM assessment derived from the current remote sensing of CDOM algorithms for riverine water is subject to large errors as compared to those for oceanic waters due to spectral signal interference from suspended sediments and chlorophyll (Del Castillo and Miller, 2008; Pan *et al.*, 2008). Therefore, remote sensing of CDOM in riverine and coastal waters remains a challenge. In such complex environments, hyperspectral remote sensing will exhibit an advantage by providing spectral responses to water inherent optical properties (IOP) in a broad spectrum of narrow bands.

Several studies confirmed that high spectral resolution (10 nm or better) improves the estimation of IOP in coastal water (Brando and Dekker, 2003; Ammenberg *et al.*, 2002; Doxaran *et al.*, 2006). However, the significant bands for CDOM estimation are not always at the same wavelengths due to the spectral signal interference from turbidity and chlorophyll, as well as the high degree of spatial and temporal heterogeneity at all scales in riverine and coastal waters. Therefore, a challenging problem in the use of hyperspectral reflectance is to identify significant wavelengths out of hundreds of narrow bands for a particular constituent (Karaska *et al.*, 2004). A common practice in analyzing hyperspectral data is to first reduce the dimensionality through band selection, derivative analysis, spectral indices, or hyperspectral transformation (Giardino *et al.*, 2007; Gong *et al.*, 2003; Pu *et al.*, 2005; Xu and Gong, 2007).

Functional linear model (FLM) has an advantage over existing approaches due to the efficient use of the abundant spectral features in hyperspectral data. This is a nonparametric method in functional data analysis (FDA) to analyze information on intrinsically smooth curves or functions (Cardot *et al.*, 2003; Cardot and Sarda, 2005). Hyperspectral reflectance across the spectrum is generally a smooth curve as a function of wavelengths. Rather than using the reflectance at all wavelengths comprehensively and equally, it is appropriate to use a functional representation to describe a spectral curve. FLM has wide applications (Ikeda *et al.*, 2008; Song *et al.*, 2008), but it has not been used for hyperspectral data analysis according to the published literature. The FLM technique has great potential for analyzing hyperspectral data and to improve IOP inversion in riverine and coastal water.

In addition to the issues of algorithms and data, the previous research on remote sensing of IOP in riverine and coastal water is usually based on a small number of ground truth samples, and is limited to satellite acquisition time and fixed locations. For example, Vignudelli *et al.* (2004) studied the distribution of DOC and CDOM in coastal waters of the northern Tyrrhenian Sea based on field data collected with a limited number of buoys. For the purpose of monitoring CDOM loading influenced by various sources from different terrestrial landscapes along a river, it is necessary to use a shipboard data acquisition approach concurrently with high spatial resolution underwater CDOM observation. However, there is little data analysis previously reported on remote sensing of CDOM calibrated and validated by concurrent high spatial resolution underwater CDOM observations.

The objective of this study is to examine if the functional linear model (FLM) would improve the analysis of hyperspectral data and reduce uncertainty in remote sensing of CDOM in rivers and tidal bays. We have conducted an underwater survey of CDOM concentrations at high spatial resolution along two rivers and a bay. A large set of *in situ* spectral reflectances was acquired above the water surface on a shipboard platform concurrently with the underwater observations. With these field measurements, we first analyze if R_{rs} can be derived accurately from total upwelling reflectance R_t acquired with a sensor viewing geometry at the nadir direction and across wide range of day time. Second, we examine if FLM could reduce the uncertainty in remote sensing of CDOM in rivers and bays which have high level of turbidity and chlorophyll. Finally, we explore the potential of using the coefficient curves of the FLM to analyze the spectral signal interference of turbidity and chlorophyll in remote sensing of CDOM.

Study Site and Data Description

Our study site encompassed the lower Hackensack and Passaic Rivers and their confluence, Newark Bay (Plate 1). This system, which is tributary to New York Harbor, contains the Port of Newark-Elizabeth Marine Terminal. The Hackensack River rises in southeastern New York. It drains the New Jersey Meadowlands, a large ecosystem of wetlands in northeast New Jersey consisting of both open, undeveloped space and developed areas, with a large proportion of natural wetlands. The Hackensack River is approximately 87 km long and has a drainage area of approximately 137 km^2. The tidal portion of the river extends from its confluence with Newark Bay upstream to New Milford, New Jersey, a distance of approximately 32 km. The Passaic River is the other tributary to Newark Bay. The river is approximately 129 km long and is tidal through the 27 km stretch from its confluence with Newark Bay upstream to the Dundee Dam in Garfield, New Jersey. However, the percentage of wetland area in the Passaic River watershed is not as large as that in the Hackensack River watershed. The depth of the Hackensack and Passaic Rivers generally ranges from 12 to 14 m, but is as deep as 61 m in places (Freeman, 1991). The mean water elevation is 0.6 m above sea level, and the average range in tide is about 1.2 m.

Methods

Several key techniques used in this study can be widely adopted by broad applications of remote sensing in water quality assessment. We describe these methods in four sections: underwater CDOM measurement, *in situ* hyperspectral measurement, removal of water-surface reflected radiance, and functional data analysis.

Underwater CDOM Measurement

Spatial variation of CDOM concentration was measured underwater on a cruise from freshwater in upper end of both the Hackensack River and the Passaic River extending seaward to Newark Bay on 24 October 2006. The MiniShuttle, a small towed vehicle based on a 0.6 m V-Fin depressor vane manufactured by YSI/Endeco was used on this survey cruise (Gardner *et al.*, 2005). A CDOM fluorometer, a chlorophyll fluorometer and an optical backscatter sensor (OBS) manufactured by Seapoint Sensors (Exeter, New Hampshire) were mounted on the MiniShuttle, as well as a 5 cm diameter MicroCTD from Falmouth Scientific (Falmouth, Massachusetts) for temperature, salinity and depth measurements. It was deployed from a 7.6 m research boat with a towing speed of about 5 kts (2.5 m/s). The instruments are able to resolve variations in CDOM fluorescence within the top 0.5 to 2 m of the water column, with horizontal sampling interval of 1 to 5 m.

The output from the CDOM fluorometer is a voltage proportional to the fluorescence at 440 nm with an excitation at 370 nm. It is necessary to convert CDOM fluorescence (voltage) to CDOM concentration (QSU). QSU denotes quinine sulfate units, which is equivalent to the fluorescence of the

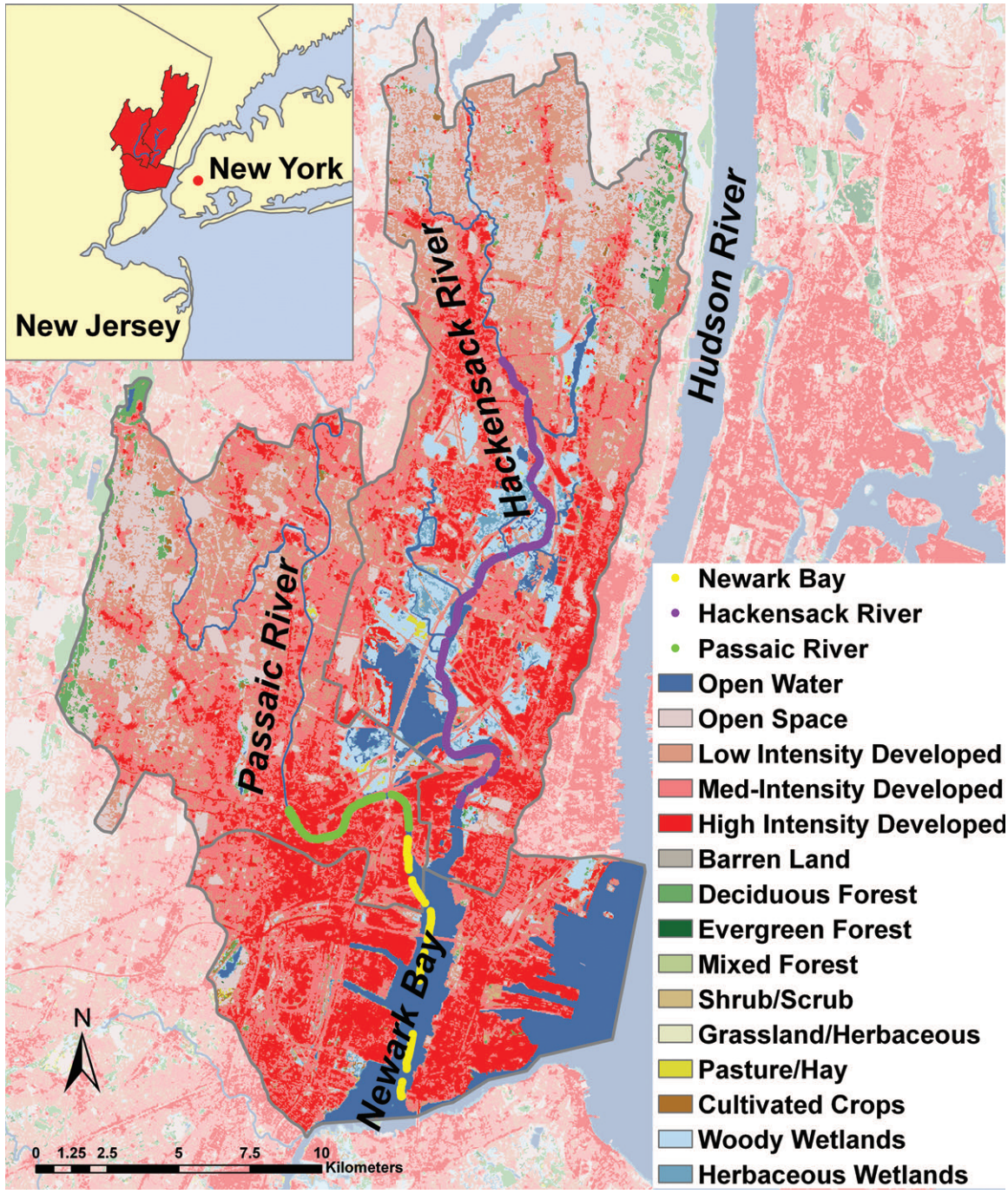

Plate 1. Study site: Passaic River, Hackensack River and Newark Bay. The dots (might be connected at this scale) in green, yellow, and pink colors are the sample points where the *in situ* hyperspectral measurements were acquired.

stated concentration of quinine dihydrogen sulfate dihydrate in 0.05 M sulfuric acid. In order to determine the CDOM concentration, we collected discrete samples in pre-combusted Pyrex bottles by hand at locations shallower than 25 cm deep in water. These discrete samples were analyzed on a Photon Technologies International (PTI) Quantum Master 1 spectrofluorometer with λ_{ex} = 337 nm, a 1 cm quartz cell, and emission scans from 350 nm to 650 nm. A blank (Milli-Q water) spectrum was subtracted from sample spectra to remove the Raman scattering peak. Fluorescence spectra were integrated in the wavelength range of 350 to 650 nm and expressed as quinine sulfate units (QSU) by computing with a five-point quinine sulfate standard curve (pH = 2) (Chen and Gardner, 2004). One QSU was equivalent to the fluorescence of 1 μg/l quinine sulfate at pH2. Discrete samples were taken from similar water masses as that recorded by the instruments for field CDOM fluorescence. With these field measurements and laboratory processes, we

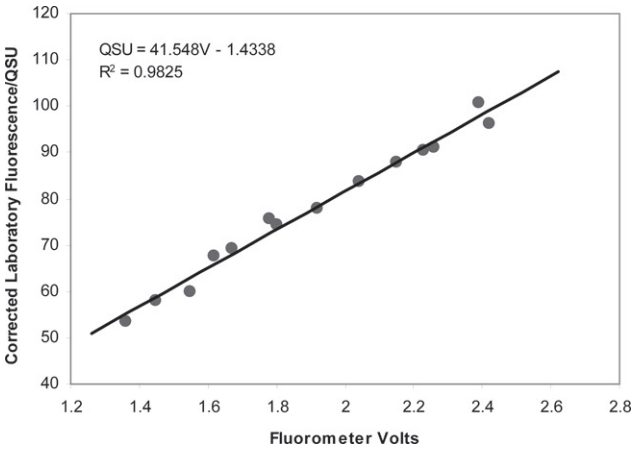

Figure 1. Correlation between Fluorometer Volts measured below water surface by MiniShuttle and corrected laboratory Fluorescence (QSU) that represents for CDOM concentration.

established a linear relationship (Figure 1) between CDOM fluorescence (voltage) and CDOM concentration (QSU). The linear function is consistent with that reported by Huang and Chen (2009) and Gardner *et al.* (2005). Because of the steady linear relationship, it is appropriate to use CDOM fluorescence (voltage) to represent CDOM concentration. In the rest of this paper, we express CDOM concentration as the fluorometer voltage.

In situ Hyperspectral Measurement

Concurrently with the underwater CDOM observations, we acquired *in situ* hyperspectral reflectance data using an Analytical Spectral Devices (ASD) spectroradiometer at 1.5 m above the water surface. The instrument uses three separate detectors spanning the visible, near-infrared (VNIR), and shortwave infrared (SWIR1 and SWIR2) with a spectral sampling interval of 1.4 nm for the VNIR detector and 1.0 nm for the SWIR detectors. The spectral measurement is resampled and reported for every 1 nm. The exploratory analysis of R_{rs} for CDOM in this project focuses on wavelengths in the range of 350 to 700 nm, where CDOM exhibits distinct optical properties. Therefore, it maintains a 351-band spectral curve for each sample point. The ASD spectroradiometer was mounted on the bow of the boat. It is equipped with a 5 m fiberoptic cable so that the sensor foreoptic can reach beyond the boat edge by more than 3 m to avoid boat shadow effects at most of boat moving directions. The majority of *in situ* remote sensing samples were acquired from 09:30 to 11:00 am and from 2:00 to 4:30 pm local time on 24 October 2006. About 5 percent of the samples were taken between 11:00 am to 2:00 pm to test if the errors introduced near Noontime can be corrected with HydroLight model. The samples were logged with concurrent GPS positions. The ASD spectroradiometer was calibrated and optimized every ten minutes or whenever cloud conditions changed. Field spectra acquisition spanned 20.6 km in the lower Hackensack River (337 samples), 6.6 km in the lower Passaic River (206 samples), and 9.5 km (141 samples) in Newark Bay (Plate 1).

Sensor viewing geometry is an important issue in remote sensing of ocean color (Maselli *et al.*, 2009). The viewing geometry is usually defined by the zenith angle θ_v, and azimuth angle φ_v. HydroLight simulations suggest that a viewing direction of 40° from the nadir (θ_v) and 135° from the Sun (φ_v) will minimize the effects of Sun glitter while avoiding instrument shading problems (Mobley, 1999). This view geometry setting is practical for stationary measurement in ocean study. However, when conducting *in situ* measurements on a shipboard platform in a cruise along a meandering river, we need to avoid the varying azimuth angle (φ_v), caused by the change in the boat heading. Although the variation of the φ_v can be minimized by using specific instruments and frequent justification, this setting would be impractical to many research projects involving mobile high resolution measurements along cruise tracks. Instead, a view geometry setting without changing φ_v is preferred. This viewing geometry can be set as perpendicular to the water surface (nadir view direction) in a boat cruise. In this way, it could avoid inconsistent φ_v, but with a trade-off of more sun glitter interference or increased surface reflected radiance. Fortunately, the trade-off effects can be minimized in post-processing using the HydroLight model (Mobley, 1999). Therefore, we conducted a series of *in situ* hyperspectral measurements using ASD spectroradiometer and acquired total water reflectance (R_t) with a viewing direction of 0° from the nadir ($\theta_v = 0$). The solar zenith angle, θ_s, was in the range of 52 to 77° during the data acquisition cruise. Although Mobley (1999) reported that surface reflectance factor has little variation for the sensor view (zenith) angles θ_v between 0 to 45° when $\theta_s > 60°$, we still verified the remote sensing reflectance R_{rs} derived from $\theta_v = 0$ setting.

Removal of Water Surface Reflected Radiance

The optical signal commonly used in ocean color is R_{rs}, in sr^{-1}. Estimation of R_{rs} from the total upwelling reflectance R_t requires three separate measurements on radiance: L_t, L_s, and L_g (Mobley, 1999):

$$R_{rs} = \frac{(L_t - \rho L_s)}{E_d} \tag{1}$$

where L_t is the total upwelling radiance reaching the detector, and L_s denotes the incident sky radiance. The sensor pointing direction for measuring L_s ($\theta_v = 180°$) is in the opposite direction to that for measuring L_t ($\theta_v = 0°$). Here, ρ is the proportionality factor that relates the L_s to water-surface reflected radiance (L_r). E_d (W m^{-2} nm^{-1}) is the downwelling irradiance incident on the water surface. E_d was estimated by radiance measurement L_g received from a spectralon white surface (Lambertian reflector) which has a known irradiance reflectance R_g as:

$$E_d(\lambda) = \frac{\pi L_g(\lambda)}{R_g(\lambda)}. \tag{2}$$

The total water surface upwelling reflectance (R_t) is defined by ASD spectroradiometer as $R_t = \frac{L_t}{L_g}$. With Equation 1 and Equation 2, R_{rs} can be estimated with the formula below

$$R_{rs}(\lambda) = R_t(\lambda)\frac{R_g(\lambda)}{\pi} - \frac{\rho L_s(\lambda)}{E_d(\lambda)} \tag{3}$$

By using HydroLight, we simulated ρ for every 30 minutes of the cruise; ρ is a function of wind speed, visibility, cloud, humidity, solar zenith angle, and sensor viewing direction. Solar zenith angles were determined by time, date, and location. Other required inputs for calculating ρ in the HydroLight model were from the NOAA National Climatic Data Center. Alternative to Equation 2, it is common to

simulate irradiance (E_d) and sky radiance (L_s) as recommended in NASA Ocean Optics Protocols (Mueller *et al.*, 2003), instead of using in situ measurements. In this study, we derived R_{rs} with the Equation 3 by using observed R_t, and simulated L_s, ρ, and E_d with the HydroLight model. The simulated parameters were validated by using 60 observed downwelling sky radiances L_s' and irradiances E_d'. If R_{rs}' denotes the remote-sensing reflectance when the Equation 3 is calculated with observed sky radiance L_s' and irradiance E_d', the uncertainty of R_{rs} can be evaluated by comparing with R_{rs}'. Our measurements for L_s' and E_d' were arranged with even time intervals (09:14 am, 10:01 am, 2:51 pm, and 3:36 pm).

Functional Data Analysis

A functional linear model was applied to improve CDOM estimation from hyperspectral R_{rs} in a spectral range of 350 to 700 nm. Generally, R_{rs} is a smooth curve corresponding to wavelengths. So the first step in developing a functional linear model is to represent each $R_{rs}(\lambda)$ by a smooth function that results from a mathematical approximation of curves using a linear combination of a set of basis functions. Example basis functions include polynomials and Fourier series. The coefficients of the linear combination were obtained through the standard least squares regression. Spline is the most preferable and common choice of polynomial basis function for nonperiodic functional data. A spline function is usually formed by joining polynomials of specified order at fixed points (Cardot *et al.*, 2003). It achieves the rapid computation of polynomials and substantially greater flexibility with only a modest number of basis functions. The B-spline is the most popular basis system to construct a spline function. A B-spline is a spline function that has minimal support with respect to a given degree, smoothness, and domain partition.

In classical statistics, a conventional multivariate linear model predicts dependent variable Y by multiple independent variables X_j in the form of

$$y_i = \alpha + \sum_j \beta_j x_{ij} + \varepsilon_i \tag{4}$$

where β_j is the regression coefficient, α is the intercept, and ε_i is the residual. Given that the independent variables are functional, a functional linear model replaces the regression coefficients by a regression coefficient function $\beta(s)$, so the model takes the form:

$$y_i = \alpha + \int_0^w x_i(s)\beta(s)ds + \varepsilon_i. \tag{5}$$

In our research context, y_i is the CDOM concentration of sample i and $x_i(s)$ is the smoothed remote sensing reflectance of sample i at wavelength s, obtained from the previous step. In order to consider the influence of individual environmental conditions in the two rivers and the bay, we introduced two dummy variables str_1 and str_2 to the FLM:

$$y_i = \alpha + \int_0^w x_i(s)\beta(s)ds + \delta_1 str_1 + \delta_2 str_2 + \varepsilon_i \tag{6}$$

If $str_1 = 1$ and $str_2 = 0$, samples were from the Hackensack River; if $str_1 = 0$ and $str_2 = 1$, samples were from the Passaic River, and if in the Newark Bay, $str_1 = 0$ and $str_2 = 0$. When these dummy variables become significant in the modeling result, it demonstrates that the spectral characteristics vary with different environmental conditions for the given field CDOM concentration. In other words, additional to spectral variables, dummy variables might improve CDOM estimation significantly.

In the estimation of the function β, the aim is not only to maintain the fidelity to the observed data, but also to avoid excessive local fluctuation. The former is measured by the residual sum of squares; the latter can be quantified by linear differential operators, such as the second order derivative. Therefore, we adopted a roughness penalty approach, penalized residual sum of squares, defined as:

$$PENSSE = \sum_{i=1}^{N}\left[y_i - \alpha - \int_0^w x_i(s)\beta(s)ds - \delta_1 str_1 - \delta_2 str_2\right]^2 + \lambda \int_0^w [D^2\beta(s)]^2 ds \tag{7}$$

A smoothing parameter λ is chosen to control the trade-off between roughness and infidelity. The larger the value of λ, the smoother the regression coefficient function $\hat{\beta}(s)$. Eventually, λ is determined as the value for which the prediction error is the lowest based on cross-validation (Figure 2). The functional data model was implemented using the statistical package R (Ramsay and Silverman, 2005).

Results and Discussion

Uncertainty Analysis of R_{rs}

Figures 3 to 5 are the uncertainty analysis of R_{rs} derived from R_t. The samples of R_t were acquired across the wide range of day time. The percent of water surface reflectance over the total upwelling reflectance, $(R_t - R_{rs})/R_t$, is about 70 to 80 percent (Figure 3). The water surface reflectance is higher at near Noontime (12:50 pm for daylight saving time) than that after 2:50 to 3:50 pm (Figure 3). The variation of surface reflectance from morning to late afternoon is less than 10 percent of the total upwelling reflectance. The small

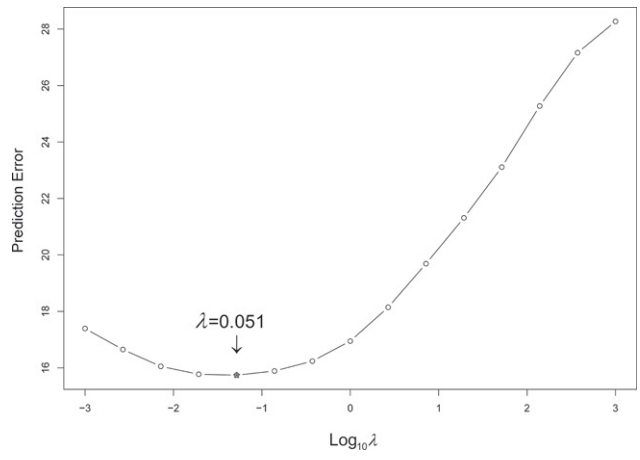

Figure 2. The smoothing parameter controls the trade-off between roughness and infidelity. The larger λ produces the smoother coefficient curve. The model determines the λ when it gives the lowest prediction error.

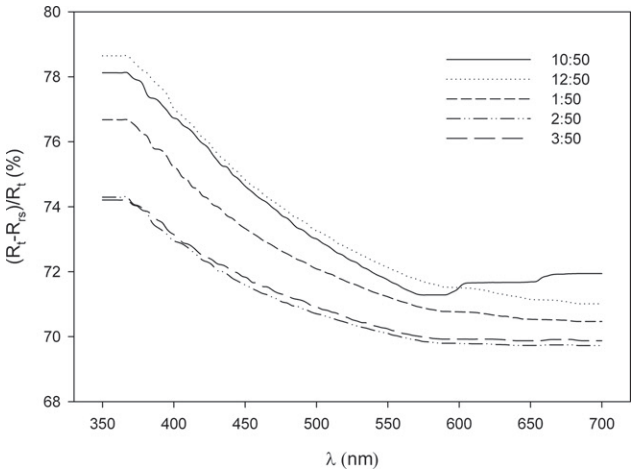

Figure 3. Percent mean of water surface reflectance over total upwelling reflectance $(R_t - R_{rs})/R_t$ across the spectrum (slightly smoothed). The samples were taken from 10:50 am to 3:50 pm at hourly intervals.

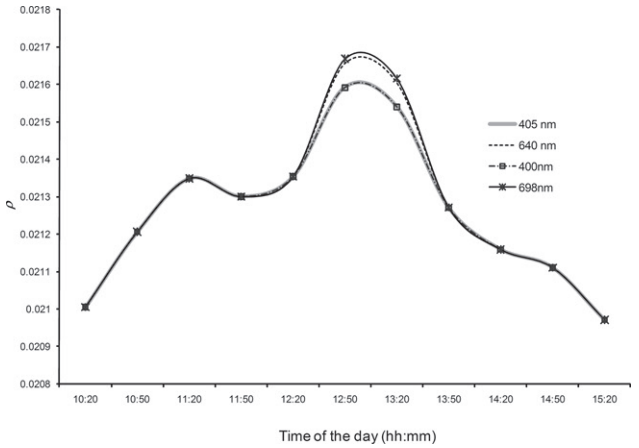

Figure 4. The variation of ρ values during the cruise at wavelengths: 400 nm, 405 nm, 640 nm, and 698 nm, respectively, for every 30 minutes.

differences across the wide range of day time confirm that we have derived R_{rs} by removing water surface reflectance from the total upwelling reflectance appropriately, including the acquisition around Noontime.

The most important parameter in removing surface reflectance is the value of ρ, the ratio of L_r to L_s. ρ was simulated with the HydroLight for every 30 minutes. Figure 4 is the variation of ρ values during the cruise at wavelengths, 400 nm, 405 nm, 640 nm, and 698 nm. It demonstrates that the ratio of L_r to L_s peaks around Noontime (1:00 pm for daylight saving time). The ratio sharply decreases when it is away from Noon. The ratio is higher at longer wavelengths (e.g., 640 nm and 698 nm) than that at shorter wavelengths (e.g., 400 nm and 405 nm) during Noontime. However, the amount of water surface reflected radiance is still higher at shorter wavelength during Noontime (Figure 3). The combination of Figure 3 and 4 revealed that shorter wavelength has

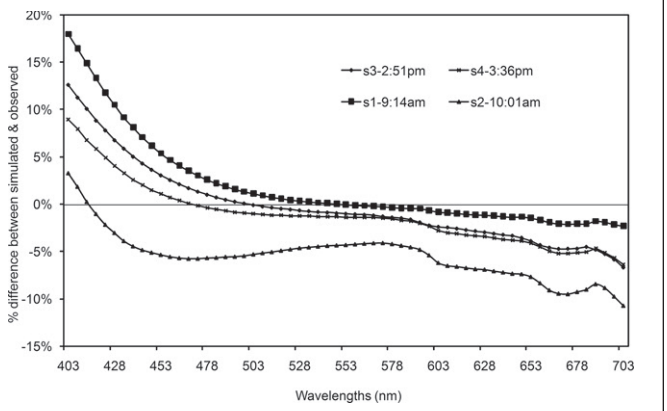

Figure 5. Differences between R_{rs} and R_{rs}', where R_{rs}' denotes the remote-sensing reflectance calculated with observed sky radiance L_s' and irradiance E_d'. This shows the uncertainty of R_{rs} by comparing with R_{rs}'.

much higher sky downwelling radiance than longer wavelengths during Noontime. This analysis provides evidence that the simulated ρ values are able to capture the higher water surface reflected radiance during noontime and the variation across the spectrum. This result indicates that *in situ* hyperspectral measurements between 11:30 am and 1:30 pm are still valuable if the values of ρ can be assessed appropriately.

In addition to ρ, two other parameters, L_s and E_d are also important factors to derive reliable R_{rs}. Figure 5 shows the uncertainty analysis of remote sensing reflectance by comparing remote sensing reflectance R_{rs}' (calculated with observed sky radiance L_s' and irradiance E_d') and R_{rs} (calculated with HydroLight simulated sky radiance L_s and irradiance E_d). The differences between R_{rs} and R_{rs}' ($R_{rs} - R_{rs}'$) across time are all less than ± 10 percent of R_{rs}, except for a few bands at very short wavelengths (403 to 428 nm). The small uncertainty exhibits that HydroLight simulated ρ, L_s, and E_d are satisfactory variables for removing surface reflected radiance from the total upwelling reflectance. Note that the R_{rs} seems slightly overestimated at shorter wavelengths and underestimated in longer wavelengths (Figure 5). All these *in situ* measurements of total upwelling reflectance R_t were acquired at a nadir-viewing direction. This uncertainty analysis confirmed that remote sensing reflectance R_{rs} derived from total upwelling reflectance R_t acquired following our shipboard setting has satisfactory quality for CDOM estimation.

CDOM Estimation using Functional Linear Model

Separate FLMs were developed to estimate CDOM in the Hackensack River, the Passiac River and Newark Bay. The model for Newark Bay provided the best estimation (Figure 6a) to underwater observations ($R^2 = 0.911$; RMSE = 0.0206) among the two rivers and the bay. The best estimation in Newark Bay coincided with small variation of turbidity in spite of relatively high value (2.6 to 2.8 OBS volts). Also the bay has low level and small variation of chlorophyll (0 and 0.2 fluorometer volts) (Figure 7). The combination of small variation of turbidity and low chlorophyll created less complexity of spectral signal interference so that the model is able to explain more CDOM variation. The data samples acquired in the Passaic River showed the similar level of turbidity and chlorophyll except slightly wider variation in turbidity

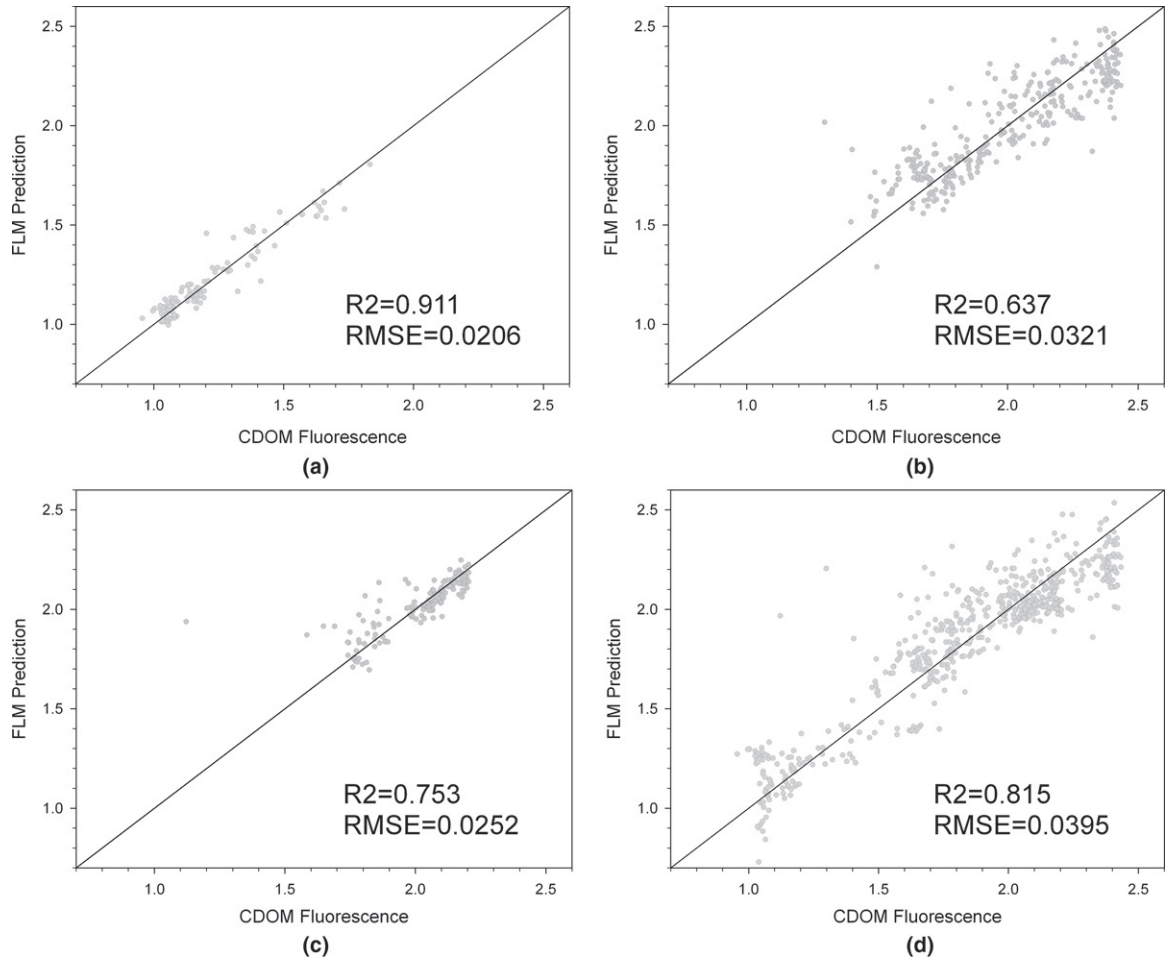

Figure 6. CDOM estimation from functional linear model for: (a) Newark Bay (R^2 = 0.911), (b) Hackensack River (R^2 = 0.637), (c) Passaic River (R^2 = 0.753), and (d) all study site (R^2 = 0.815).

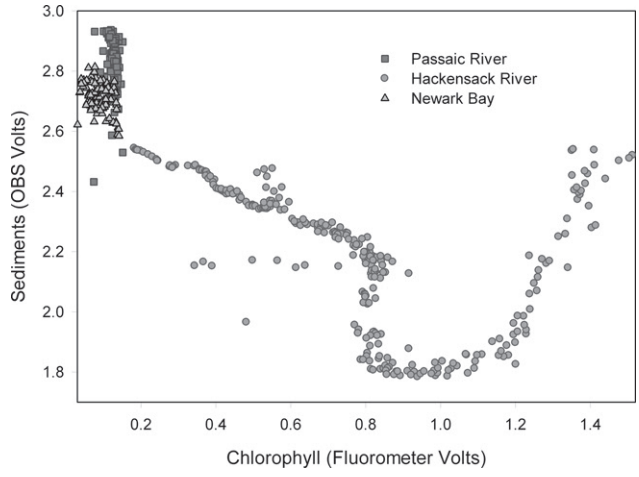

Figure 7. The range of turbidity and chlorophyll in the two rivers and the bay.

(2.4 to 3.0 OBS volts) compared to Newark Bay (Figure 7). The FLM for the Passaic River did not predict CDOM (R^2 = 0.753, and RSME = −0.0252) as well as that for the Newark Bay (Figure 6c).

The levels of chlorophyll and turbidity in the Hackensack River were in much broader ranges compared to that in both Newark Bay and the Passaic River (Figure 7). Since turbidity and chlorophyll cause spectral signal interferences, the model for the Hackensack River did not explain CDOM variation (R^2 = 0.64, RSME = 0.0321) as well as that for the Passaic River and Newark Bay (Figure 6). In fact, none of the published remote sensing algorithms (Lee and Hu, 2006) could explain more than 50 percent the variations of CDOM observations in riverine and coastal water. In spite of the variations of turbidity and chlorophyll levels, the FLM for the Hackensack River still produced a satisfactory CDOM estimation. The functional linear models have indicated an apparent advantage in reducing uncertainty of remote sensing of CDOM in riverine and coastal water over existing algorithms. The advantage is attributed to the fact that the FLM is able to take into account the abundant hyperspectral features in a broad spectrum, which capture the shifts of wavelengths significant to CDOM analysis

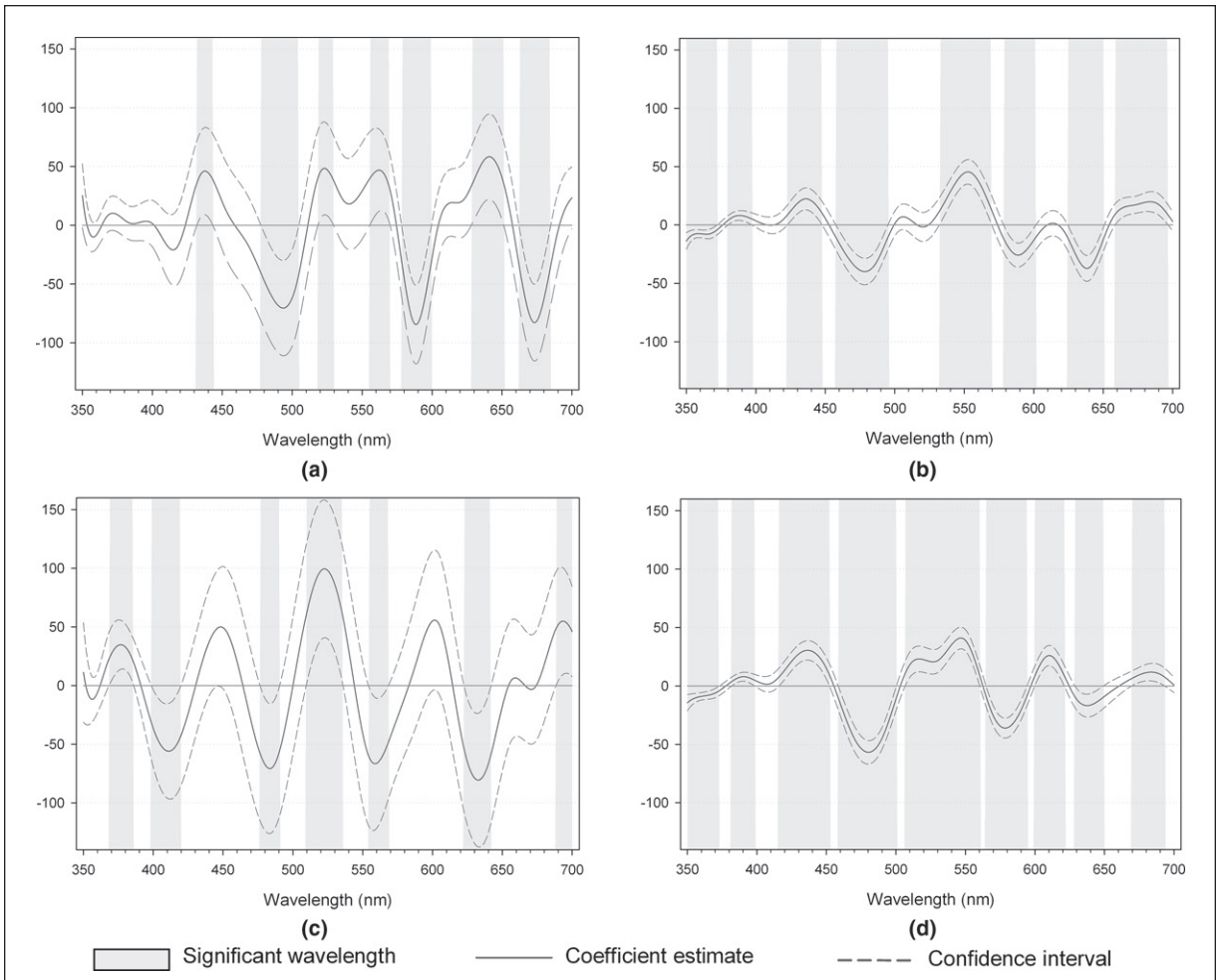

Figure 8. Coefficient curves of the functional linear model for: (a) Newark Bay (R^2 = 0.911), (b) Hackensack River (R^2 = 0.637), (c) Passaic River (R^2 = 0.753), (d) all study site (R^2 = 0.815). The curves in solid lines plot the coefficients of models developed for each scenario (two rivers, a bay, and lumped scenario). The two dashed lines above and below each coefficient curve denote the confidence intervals. A wavelength is considered significant if the confidence interval of the corresponding coefficient does not include zero. The further a coefficient and its confidence interval are away from zero, the more significant the corresponding wavelength is. The regions shaded in gray are significant wavelength regions.

(Figure 8). The shifts of significant wavelengths are usually caused by the high variation of turbidity and chlorophyll levels. These evidences confirmed that the variation of turbidity and chlorophyll affects remote sensing of CDOM (Kahru and Mitchell, 2001).

Linear functional modeling results indicated that the variation of environmental conditions in individual river watershed is a major determinant of riverine CDOM concentration. For example, both modeled and observed CDOM concentrations in the Hackensack River are clustered to the high end (Figure 6b). The Hackensack River is bordered by extensive tidal wetlands and open water areas, while the Passaic River is mainly surrounded by developed areas. The high CDOM concentration in the Hackensack River coincided with the high percentage of wetland and salt-marsh areas in the river watershed (Plate 1). This is consistent with the results from many previous studies (Aitkenhead *et al.*, 1999; Gardner *et al.*, 2005). The large fluxes of CDOM occur when wetlands serve as barriers precluding water infiltration of the soil column. Because of the river-wetland interaction, the Hackensack River also has greater variation of CDOM concentrations than either the Passaic River or Newark Bay. CDOM concentrations in both the Passaic River and the Hackensack River are much higher than that in Newark Bay, where the level of salinity is much higher and the terrigeneous CDOM was diluted by marine water.

The influences of local environmental factors on riverine CDOM became clear in a lumped scenario in which all data from the two rivers and the bay were merged. The FLM for the lumped scenario explained about 81.5 percent (RMSE = 0.0395) of the underwater CDOM variation (Figure 6d). Since about 50 percent data in the scenario are from the Hackensack River, the wide variation of turbidity and chlorophyll levels affected the FLM. This situation is common when a FLM is applied to multiple rivers. Additionally, the model for the lumped scenario was further improved by adding two dummy variables indicating the influence of location characteristics of two rivers and the bay (Equation 6 and 7).

TABLE 1. COEFFICIENTS AND CONFIDENCE INTERVALS OF TWO DUMMY VARIABLES AND THE CONSTANT (INTERCEPT) OF THE FUNCTIONAL LINEAR MODEL

	Coefficient δ/ Intercept α	Lower Conf. Interval	Upper Conf. Interval
Hackensack ($str_1 = 1$, $str_2 = 0$)	4.77×10^{-3}	4.60×10^{-3}	4.93×10^{-3}
Passaic ($str_1 = 0$, $str_2 = 1$)	5.08×10^{-3}	4.94×10^{-3}	5.20×10^{-3}
Newark Bay ($str_1 = 0$, $str_2 = 0$)	3.68×10^{-3}	3.49×10^{-3}	3.88×10^{-3}

The resultant coefficients of the dummy variable for the Hackensack River ($str_1 = 1$, $str_2 = 0$) and the Passaic River ($str_1 = 0$, $str_2 = 1$) were $\delta_1 = 4.77 \times 10^{-3}$ and $\delta_2 = 5.08 \times 10^{-3}$, respectively, as listed in Table 1. Because the confidence intervals of δ_1 and δ_2 do not include zero, they are both statistically significant in the model. The statistical significance indicates the uniqueness of environmental conditions in the Hackensack River and in the Passaic River. The model improved the estimation by 3 percent ($R^2 = 0.84$), if the dummy variables were considered. This result demonstrates that local environmental factors have impacts on the relationship between CDOM and spectral curves. Some field studies have shown that the optical properties of CDOM at a given concentration vary slightly due to different sources, production and regulation (Aitkenhead-Peterson *et al.*, 2003). For example, the autochthonous CDOM (derived from algae and macrophytes) will look lighter than allochthonous CDOM (derived from organic soil and humic substances). Wang *et al.* (2010) reported that the potential environmental factors associated with the CDOM sources are surface and ground water runoff, vegetation characteristics and density, and soil properties.

Furthermore, the positive coefficients for the two dummy variables suggested that the FLM would underestimate the CDOM in rivers by neglecting the differences in local environmental conditions. The FLM has the advantage of including ancillary information in addition to spectral signatures. It implied that remote sensing of CDOM can be potentially improved by including some variables representing local environments, such as percentage of vegetation cover in the watershed.

Variation of FLM Coefficient Curve

The functions or curves of the FLM coefficients provided intuitive information on the most significant wavelengths for remote sensing of CDOM (Figure 8). By comparing the significant wavelengths among the four scenarios (two rivers, the bay, and lumped data), we noticed that coefficient curves vary in: (a) magnitude of coefficients, (b) range of confidence intervals, (c) the number of significant regions (the number of peaks or troughs in a curve), and (d) peak wavelength positions in each of four scenarios. The coefficient curves for Newark Bay (Figure 8a) and the Passaic River (Figure 8c) have a similar pattern in terms of high magnitude and wider range of confidence intervals. This pattern is consistent with their similar environmental conditions: low chlorophyll and high level of turbidity (Figure 7). The high turbidity level was caused by the transit of cargo ships to several ports and to industrial locations in the Newark Bay channel (e.g., the port of Newark-Elizabeth Marine Terminal) as well as the lower Passaic River (Kruger, 2008). In contrast, the coefficient curves for the Hackensack River (Figure 8b) and for the lumped scenario (Figure 8d) share a pattern of smaller magnitude and confidence intervals. This curve pattern is consistent with the relatively low turbidity and the wide variation of chlorophyll in the Hackensack River (Figure 7).

Based on the above pattern analysis, we conjecture that the variations of the coefficient curves for CDOM estimation are mainly degraded by spectral signals of turbidity and chlorophyll as their quantities greatly affect water optical properties (Han, 1997; Rundquist *et al.*, 1996). It appears that the pattern representing Newark Bay (Figure 8a) and the Passaic River (Figure 8c) was influenced by the high turbidity (Figure 7). The absorption by tripton (detrital particles) in water is low at the red end of the spectrum and rises steadily as wavelength decreases into the blue and ultraviolet. Contrarily to absorption, tripton increases the reflectance at the wavelengths of 570 to 690 nm (Chen *et al.*, 2009; Chen *et al.*, 2007; Fraser, 1998; Hadjimitsis *et al.*, 2006). Due to the spectral scattering and absorption interferences from the mineral dominated turbidity in Newark Bay and the Passaic River, the shape of FLM coefficient curves for CDOM estimation is different from that with low turbidity and high chlorophyll conditions in the Hackensack River (Figure 8b).

For the two high turbidity scenarios, the coefficient curves have several local maxima and minima at wavelengths in the spectral region from 570 nm to 690 nm. Also, confidence intervals of the coefficient curves for the high turbidity scenarios are much larger than that in the Hackensack where turbidity level is lower and chlorophyll is higher. In any case, soil types in watersheds contributing to the turbidity in riverine and coastal water would make significant difference in both reflectance magnitude and peak shift (Lodhi *et al.*, 1997). When turbidity is influenced by various levels of soil suspended sediment concentrations, the coefficient curves would be far more complex than what we observed in this project. The potential relationship between coefficient curves and turbidity level indicated that there is great need for more observation data to quantitatively examine the spectral interference of turbidity to CDOM estimation.

It seams that the patterns of coefficient curves for the Hackensack River (Figure 8b) and the lumped scenario (Figure 8d) were largely influenced by the spectral characteristics of chlorophyll at wavelengths of 400 to 700 nm. Chlorophyll-*a* and -*b* absorb blue light centered at 430 nm and 450 nm and red light centered at 660 nm and 650 nm (Jensen, 2007). Because of the lower absorption of green light, chlorophyll causes the reflectance maximum around 550 nm (green peak). Also there is a prominent reflectance peak around 690 to 700 nm caused by an interaction of algal-cell scattering (Rundquist *et al.*, 1995). The varying levels of chlorophyll change the magnitude of the local maxima and minima at either the exact or slightly shifted wavelengths (Figure 8b and 8d). For the Hackensack River, minima occur at 435 nm, 475 nm, and 640 nm; maxima occur at 550 nm and 690 nm (Figure 8b). Other significant wavelengths at 390 nm and 590 nm have relatively small magnitude. This change suggests chlorophyll interference to remotely estimated CDOM distribution (Lee *et al.*, 1994; Carder *et al.*, 2002; SCCF RECON, 2008).

Our analysis demonstrated the advantages of using a functional linear model over an ordinary linear regression model. First, FLM produces better CDOM estimation by using spectral features at more or all wavelengths. FLM

approximates spectral reflectance curves by linearly "stacking" a modest number of predefined basis functions (65 B-spline of order 4) rather than the large number of bands in an ordinary linear model (351 bands). The reduced number of variables allows much less field observations to construct the FLM and solve the regression coefficients. Second, the estimate of regression coefficients is a continuous smooth functional curve of wavelength. The smoothed functional coefficients prevent the model from over-fitting the observed data. The coefficient function curve provides much more intuitive information on the relative significance of each individual wavelength of hyperspectral data in CDOM estimation. We believe these advantages of using FLM can improve a wide range of applications using hyperspectral remote sensing.

Conclusions

Based on a large set of high spatial resolution underwater CDOM observations and concurrent *in situ* above-surface hyperspectral measurements of the total upwelling reflectance, we examined a functional linear model approach to see if it reduces the uncertainty in remote sensing of CDOM in riverine and coastal water. Before introducing the FLM approach, we evaluated the feasibility of *in situ* remote sensing of CDOM from above-surface at nadir direction and across wide range of hours in a day. Results confirmed that the HydroLight model is efficient in removing water surface reflected radiance, allowing use of data acquired at a nadir sensor viewing angle ($\theta_v = 0$). With the support of the HydroLight model, the procedure allows shipboard data acquisition without considering the change of azimuth angle (φ_v) from a boat cruise along a meandering river.

This study concludes with several suggestions. First, the FLM is able to reduce uncertainty in remote sensing of CDOM in riverine and coastal water and outperforms existing algorithms. For the scenario of less variation of turbidity and chlorophyll, the model explained 91 percent of CDOM variation in the Newark Bay (RMSE = 0.0206). For the worst scenario of a wide range of turbidity and chlorophyll, the model is still able to predict CDOM up to 64 percent in the Hackensack River (RSME = 0.0321).

Second, the FLM has an advantage of including ancillary information in remote sensing of CDOM. The results demonstrated that CDOM estimation was improved by introducing dummy variables representing local environmental conditions. This indicated that ancillary information in addition to spectral reflectance would be helpful to CDOM assessment in riverine water.

Third, the patterns of FLM coefficient curve provide critical information of identifying different level of CDOM concentration. It also explicitly shows the spectral signal interference from turbidity and chlorophyll as their quantities greatly affect water optical properties. However, our analysis was largely based on visual assessment. Current results are not sufficient to systematically explain the causes of FLM coefficient variation across the spectrum. In future research, large stratified field observations representing a broad range of river conditions and water quality should be implemented. In this way, we can understand how the coefficient curves change corresponding to the level of turbidity and chlorophyll. With this improved understanding, we can modify the functional linear model so as to reduce uncertainty in remote sensing of CDOM in riverine and coastal water.

Acknowledgments

The study was supported by a grant of US Office of Naval Research (Grant No. N00014-3 06-10220). The authors are very grateful for the field sample collection and laboratory process provided by Francesco Peri, Wei Huang, and Kim Frashure.

References

Aitkenhead, J.A., D. Hope, and M.F. Billett, 1999. The relationship between dissolved organic carbon in stream water and soil organic carbon pools at different spatial scales, *Hydrological Processes*, 13:1289–1302.

Aitkenhead, J.A., W.H. McDowell, and J.C. Neff, 2003. Sources, production, and regulation of allchthonous dissovlved organic matter inputs to surface waters, *Aquatic Ecosystems: Interactivity of Dissolved Organic Matter* (S.E. Findlay and R.L. Sinsabaugh, editors), Academic Press, pp. 25–70.

Ammenberg, P., P. Flink, T. Lindell, D. Pierson, and N. Strombeck, 2002. Bio-optical modelling combined with remote sensing to assess water quality, *International Journal of Remote Sensing*, 23:1621–1638.

Antoine, D., F. d'Ortenzio, S.B. Hooker, G. Becu, B. Gentili, D. Tailliez, and A.J. Scott, 2008. Assessment of uncertainty in the ocean reflectance determined by three satellite ocean color sensors (MERIS, SeaWiFS and MODIS-A) at an offshore site in the Mediterranean Sea (BOUSSOLE Project), *Journal of Geophysical Research-Oceans*, 113, C07013.

Brando, V.E., and A.G. Dekker, 2003. Satellite hyperspectral remote sensing for estimating estuarine and coastal water quality, *IEEE Transactions on Geoscience and Remote Sensing*, 41(6):1378–1387.

Bricaud, A., A. Morel, and L. Prieur, 1981. Absorption by dissolved organic matter of the sea (yellow substance) in the UV and visible domains, *Limnology and Oceanography*, 26(1):43–53.

Brown, C.A., Y. Huot, P.J. Werdell, B. Gentili, and H. Claustre, 2008. The origin and global distribution of second order variability in satellite ocean color and its potential applications to algorithm development, *Remote Sensing of Environment*, 112(12):4186–4203.

Carder, K.L., F.R. Chen, J.P. Cannizzaro, J.W. Campbell, and B.G. Mitchell, 2002. Performance of the MODIS semi-analytical ocean color algorithm for chlorophyll-a, *Proceedings of the 2nd World Space Congress/34th COSPAR Scientific Assembly* (P. Schlussel, R. Stuhlmann, J.W. Campbell, and C. Erickson, editors), Houston, Texas, pp. 1152–1159.

Cardot, H., R. Faivre, and M. Goulard, 2003. Functional approaches for predicting land use with the temporal evolution of coarse resolution remote sensing data, *Journal of Applied Statistics*, 30(10):1185–1199.

Cardot, H, F. Ferraty, and P. Sarda, 2003. Spline estimators for the functional linear model, *Statistica Sinica*, 13(3):571–591.

Cardot, H., and P. Sarda, 2005. Estimation in generalized linear models for functional data via penalized likelihood, *Journal of Multivariate Analysis*, 92(1):24–41.

Chen, R.F., and G.B. Gardner, 2004. High-resolution measurements of chromophoric dissolved organic matter in the Mississippi and Atchafalaya River plume regions, *Marine Chemistry*, 89(1–4):103–125.

Chen, S.S., L.G. Fang, L.X. Zhang, and W.R. Huang, 2009. Remote sensing of turbidity in seawater intrusion reaches of Pearl River Estuary - A case study in Modaomen water way, China, *Estuarine Coastal and Shelf Science*, 82(1):119–127.

Chen, Z.Q., C.M. Hu, and F. Muller-Karger, 2007. Monitoring turbidity in Tampa Bay using MODIS/Aqua 250-m imagery, *Remote Sensing of Environment*, 109(2):207–220.

Del Castillo, C.E., F. Gilbes, P.G. Coble, and F.E. Muller-Karger, 2000. On the dispersal of riverine colored dissolved organic matter over the West Florida Shelf, *Limnology and Oceanography*, 45(6):1425–1432.

Del Castillo, C.E., and R.L. Miller, 2008. On the use of ocean color remote sensing to measure the transport of dissolved organic carbon by the Mississippi River Plume, *Remote Sensing of Environment*, 112(3):836–844.

Doxaran, D., N. Cherukuru, and S.J. Lavender, 2006. Apparent and inherent optical properties of turbid estuarine waters: Measure-

ments, empirical quantification relationships, and modeling, *Applied Optics*, 45(10):2310–2324.

Ferrari, G.M., M.D. Dowell, S. Grossi, and C. Targa, 1996. Relationship between the optical properties of chromophoric dissolved organic matter and total concentration of dissolved organic carbon in the southern Baltic Sea region, *Marine Chemistry*, 55(3–4):299–316.

Fraser, R.N., 1998. Hyperspectral remote sensing of turbidity and chlorophyll a among Nebraska sand hills lakes, *International Journal of Remote Sensing*, 19(8):1579–1589.

Freeman, W.O., 1991. National Water Quality Assessment Program - The Hudson River Basin, URL: *http://ny.water.usgs.gov/projects/hdsn/fctsht/su.html*, U.S. Geological Survey, New York Water Science Center, Troy, New York (last date accessed: 14 July 2010).

Gardner, G.B., R.F. Chen, and A. Berry, 2005. High-resolution measurements of chromophoric dissolved organic matter (CDOM) in the Neponset River Estuary, Boston Harbor, Massachusetts, *Marine Chemistry*, 96(1–2):137–154.

Giardino, C., V.E. Brando, A.G. Dekker, N. Strombeck, and G. Candiani, 2007. Assessment of water quality in Lake Garda (Italy) using Hyperion, *Remote Sensing of Environment*, 109(2):183–195.

Gong, P., R.L. Pu, G.S. Biging, and M.R. Larrieu, 2003. Estimation of forest leaf area index using vegetation indices derived from Hyperion hyperspectral data, *IEEE Transactions on Geoscience and Remote Sensing*, 41(6):1355–1362.

Hadjimitsis, D.G., M.G. Hadjimitsis, C. Clayton, and B.A. Clarke, 2006. Determination of turbidity in Kourris Dam in Cyprus utilizing Landsat TM remotely sensed data, *Water Resources Management*, 20(3):449–465.

Han, L.H., 1997. Spectral reflectance with varying suspended sediment concentrations in clear and algae-laden waters, *Photogrammetric Engineering & Remote Sensing*, 63(6):701–705.

Hansell, D.A., and C.A. Carlson, 2002. *Biogeochemistry of Marine Dissolved Organic Matter*, Academic Press, Boston, 774 p.

Huang, W., and R.F Chen, 2009. Sources and transformations of chromophoric dissolved organic matter in the Neponset River Watershed, *Journal of Geophysical Research- Biogeosciences*, 114, G00F05.

Ikeda, T., M. Dowd, and J.L. Martin, 2008. Application of functional data analysis to investigate seasonal progression with interannual variability in plankton abundance in the Bay of Fundy, Canada, *Estuarine Coastal and Shelf Science*, 78(2):445–455.

Jensen, J.R., 2007. *Remote Sensing of the Environment*, Pearson Prentice Hall, Upper Saddle River, New Jersey, 544 p.

Kahru, M., and G.B. Mitchell, 2001. Seasonal and nonseasonal variability of satellite-derived chlorophyll and colored dissolved organic matter concentration in the California Current, *Journal of Geophysical Research-Oceans*, 106(C2):2517–2529.

Karaska, M.A., R.L. Huguenin, J.L. Beacham, M.H. Wang, J.R. Jensen, and R.S. Kaufmann, 2004. AVIRIS measurements of chlorophyll, suspended minerals, dissolved organic carbon, and turbidity in the Neuse River, North Carolina, *Photogrammetric Engineering & Remote Sensing*, 70(1):125–133.

Kishino, M., A. Tanaka, and J. Ishizaka, 2005. Retrieval of Chlorophyll a, suspended solids, and colored dissolved organic matter in Tokyo Bay using ASTER data, *Remote Sensing of Environment*, 99(1–2):66–74.

Kruger, A.L., 2008. Comments Regarding Lower Passaic River - Phase 1 Removal Action Engineering Evaluation/Cost Analysis, Tierra Solutions, Inc., URL: *http://www.passaicriver.org/images/LowerPassaicRestorationProject/TAG-Tierra-0812- Phase-I.pdf*, Passaic River Coalition (last date accessed: 14 July 2010).

Kutser, T., D.C. Pierson, L. Tranvik, A. Reinart, S. Sobek, and K.Y. Kallio, 2005a. Using satellite remote sensing to estimate the colored dissolved organic matter absorption coefficient in lakes, *Ecosystems*, 8(6):709–720.

Kutser, T., D.C. Pierson, K.Y. Kallio, A. Reinart, and S. Sobek, 2005b. Mapping lake CDOM by satellite remote sensing, *Remote Sensing of Environment*, 94(4):535–540.

Lee, Z.P., K.L. Carder, S.K. Hawes R.G. Steward, T.G. Peacock, and C.O..Davis, 1994. Model for the interpretation of hyperspectral remote-sensing reflectance, *Applied Optics*, 33(24):5721–5732.

Lee, Z.P., K.L. Carder, and R. Arnone, 2002. Deriving inherent optical properties from water color: A multi-band quasi-analytical algorithm for optically deep water, *Applied Optics*, 41(27):5755–5772.

Lee, Z.P., and C.M. Hu, 2006. Global distribution of Case-1 waters: An analysis from SeaWiFS measurements, *Remote Sensing of Environment*, 101(2):270–276.

Lodhi, M.A., D.C. Rundquist, L.H. Han, and M.S. Kuzila, 1997. The potential for remote sensing of loess soils suspended in surface waters, *Journal of the American Water Resources Association*, 33(1):111–117.

Mannino, A., M.E. Russ, and S.B. Hooker, 2008. Algorithm development and validation for satellite-derived distributions of DOC and CDOM in the US Middle Atlantic Bight, *Journal of Geophysical Research-Oceans*, 113, C07051.

Maselli, F., L. Massi, M. Pieri, and C. Santini, 2009. Spectral angle minimization for the retrieval of optically active seawater constituents from MODIS data, *Photogrammetric Engineering & Remote Sensing*, 75(5):595–605.

Mobley, C.D., 1999. Estimation of the remote-sensing reflectance from above-surface measurements, *Applied Optics*, 38(36):7442–7455.

Mueller, J.L., and R.W. Austin, 1992. *Ocean Optics Protocols for SeaWiFS Validation*, NASA Technical Memo. 104566, SeaWiFS Technical Report Series, NASA Goddard Space Flight Center, Greenbelt, Maryland, p. 45.

Mueller, J.L., S.W. Brown, D.K. Clark, B.C. Johnson, H. Yoon, K.R. Lykke, S.J. Flora, M.E. Feinholz, N. Souaidia, C. Pietras, T.C. Stone, M.A. Yarbrough, Y.S. Kim, and R.A. Barnes, 2003. *Ocean Optics Protocols for Satellite Ocean Color Sensor Validation, Revision 4, Volume III, Radiometric Measurements and Data Analysis Protocols* (J.L. Mueller, G.S. Fargion, and C.R. McClain, editors), NASA Technical Memo 21621, 84 p.

Pan, X.J., A. Mannino, M.E. Russ, and S.B. Hooker, 2008. Remote sensing of the absorption coefficients and chlorophyll a concentration in the United States southern Middle Atlantic Bight from SeaWiFS and MODIS-Aqua, *Journal of Geophysical Research- Oceans*, 113, C11022.

Pu, R., Q. Yu, P. Gong, and G.S. Biging, 2005. EO-1 Hyperion, ALI and Landsat 7 ETM+ data comparison for estimating forest crown closure and leaf area index, *International Journal of Remote Sensing*, 26(3):457–474.

Ramsay, J.O., and B.W. Silverman, 2005. *Functional Data Analysis*, Springer, 426 p.

Ritchie, J.C., P.V. Zimba, and J.H. Everitt, 2003. Remote sensing techniques to assess water quality, *Photogrammetric Engineering & Remote Sensing*, 69(6):695–704.

Rundquist, D.C., J.F. Schalles, and J.S. Peake, 1995. The response of volume reflectance to manipulated algal concentrations above bright and dark bottoms at various depths in an experiental pool, *Geocarto International*, 10(4):5–14.

Rundquist, D.C., L.H. Han, J.F. Schalles, and J.S. Peake, 1996. Remote measurement of algal chlorophyll in surface waters: The case for the first derivative of reflectance near 690 nm, *Photogrammetric Engineering & Remote Sensing*, 62(2):195–200.

SCCF RECON, 2008, Colored Dissolved Organic Matter, URL: *http://recon.sccf.org/definitions/cdom.shtml* (last date accessed: 14 July 2010).

Siegel, D.A., S. Maritorena, N.B. Nelson, D.A. Hansell, and M. Lorenzi-Kayser, 2002. Global distribution and dynamics of colored dissolved and detrital organic materials, *Journal of Geophysical Research-Oceans*, 107(C12), 3228.

Song, J.J., W. Deng, H.J. Lee, and D. Kwon, 2008. Optimal classification for time-course gene expression data using functional data analysis, *Computational Biology and Chemistry*, 32(6):426–432.

Spencer, R.G.M., J.M.E. Ahad, A. Baker, G.L. Cowie, R. Ganeshram, R.C. Upstill-Goddard, and G. Uher, 2007. The estuarine mixing

behaviour of peatland derived dissolved organic carbon and its relationship to chromophoric dissolved organic matter in two North Sea estuaries (UK), *Estuarine Coastal and Shelf Science*, 74(1–2):131–144.

Stedmon, C.A., S. Markager, M. Sondergaard, T. Vang, A. Laubel, N.H. Borch, and A. Windelin, 2006. Dissolved organic matter (DOM) export to a temperate estuary: Seasonal variations and implications of land use, *Estuaries and Coasts*, 29(3):388–400.

Vignudelli, S., C. Santinelli, E. Murru, L. Nainnicini, and A. Seritti, 2004. Distributions of dissolved organic carbon (DOC) and chromophoric dissolved organic matter (CDOM) in coastal of the northern Tyrrhenian Sea (Italy), *Estuarine Coastal and Shelf Science*, 60(1):133–149.

Wang, D.W., Y.Q. Tian, and W. Huang, 2010. Using hydrology model to study DOC concentration in soil water and streams: A case study of an urban watershed in southeast of Boston, Massachusetts, *Hydrological Processses* (in review).

Xu, B., and P. Gong, 2007. Land-use/land-cover classification with multispectral and hyperspectral E0-1 data, *Photogrammetric Engineering & Remote Sensing*, 73(8):955–965.

ASPRS Code of Ethics

Honesty, justice, and courtesy form a moral philosophy which, associated with mutual interest among people, should be the principles on which ethics are founded.

Each person who is engaged in the use, development, and improvement of the mapping sciences (Photogrammetry, Remote Sensing, Geographic Information Systems, and related disciplines) should accept those principles as a set of dynamic guides for conduct and a way of life rather than merely for passive observance. It is an inherent obligation to apply oneself to one's profession with all diligence and in so doing to be guided by this Code of Ethics.

Accordingly, each person in the mapping sciences profession shall have full regard for achieving excellence in the practice of the profession and the essentiality of maintaining the highest standards of ethical conduct in responsibilities and work for an employer, all clients, colleagues and associates, and society at large, and shall . . .

1. Be guided in all professional activities by the highest standards and be a faithful trustee or agent in all matters for each client or employer.
2. At all times function in such a manner as will bring credit and dignity to the mapping sciences profession.
3. Not compete unfairly with anyone who is engaged in the mapping sciences profession by:
   a. Advertising in a self-laudatory manner;
   b. Monetarily exploiting one's own or another's employment position;
   c. Publicly criticizing other persons working in or having an interest in the mapping sciences;
   d. Exercising undue influence or pressure, or soliciting favors through offering monetary inducements.
4. Work to strengthen the profession of mapping sciences by:
   a. Personal effort directed toward improving personal skills and knowledge;
   b. Interchange of information and experience with other persons interested in and using a mapping science, with other professions, and with students and the public;
   c. Seeking to provide opportunities for professional development and advancement of persons working under his or her supervision;
   d. Promoting the principle of appropriate compensation for work done by person in their employ.
5. Undertake only such assignments in the use of mapping sciences for which one is qualified by education, training, and experience, and employ or advise the employment of experts and specialists when and whenever clients' or employers' interests will be best served thereby.
6. Give appropriate credit to other persons and/or firms for their professional contributions.
7. Recognize the proprietary, privacy, legal, and ethical interests and rights of others. This not only refers to the adoption of these principles in the general conduct of business and professional activities, but also as they relate specifically to the appropriate and honest application of photogrammetry, remote sensing, geographic information systems, and related spatial technologies. Subscribers to this code shall not condone, promote, advocate, or tolerate any organization's or individual's use of these technologies in a manner that knowingly contributes to:
   a. deception through data alteration;
   b. circumvention of the law;
   c. transgression of reasonable and legitimate expectation of privacy.